ELSEVIER

Contents lists available at ScienceDirect

Fuel

journal homepage: www.elsevier.com/locate/fuel



Full length article

Insights into site evaluation for underground hydrogen storage (UHS) on gas mixing-the effects of meter-scale heterogeneity and associated reservoir characterization parameters

Zhenkai Bo ^{a,b}, Sebastian Hörning ^a, Kunning Tang ^c, Jim R. Underschultz ^a, Suzanne Hurter ^{a,d}

- ^a Gas & Energy Transition Research Centre, University of Queensland, St Lucia, Brisbane, 4072, Queensland, Australia
- ^b Institute of GeoEnergy Engineering, Heriot-Watt University, Edinburgh, EH14 4AS, United Kingdom
- c School of Minerals and Energy Resources Engineering, The University of New South Wales, Kengsington, Sydney, 2052, New South Wales, Australia
- ^d TNO, Applied Geosciences, Princetonlaan 6, Utrecht, The Netherlands

ARTICLE INFO

Keywords: Underground Hydrogen Storage Gas mixing Metre-scale heterogeneity Flow diagnostics

ABSTRACT

Underground Hydrogen Storage (UHS), as an emerging large-scale energy storage technology, has shown great promise to ensure energy security with minimized carbon emission. A set of comprehensive UHS site evaluation criteria based on important factors that affect UHS performances is needed for its potential commercialization. This study focuses on the UHS site evaluation of gas mixing. The economic implications of gas mixing between injected hydrogen gas and the residual or cushion gas in a porous storage reservoir is an emerging problem for Underground Hydrogen Storage (UHS). It is already clear that reservoir scale heterogeneity such as formation structure (e.g. formation dip angle) and facies heterogeneity of the sedimentary rock may considerably affect the reservoir-scale mechanical dispersion-induced gas mixing during UHS in high permeability braided-fluvial systems (a common depleted reservoir type for UHS). Following this finding, the current study uses the process-mimicking modeling software to build synthetic meandering-fluvial reservoir models. Channel dimensions and the presence of abandoned channel facies are set as testing parameters, resulting in 4 simulation cases with 200 realizations. Numerical flow simulations are performed on these models to investigate and compare the effects of reservoir and metre-scale heterogeneity on UHS gas mixing.

Through simulation, channel dimensions (reservoir-scale heterogeneity) are found to affect the uncertainty of produced gas composition due to mixing (represented by the P10-P90 difference of hydrogen fraction in a produced stream) by up to 42%. The presence of abandoned channel facies (metre-scale heterogeneity), depending on their architectural relationship with meander belts, could also influence the gas mixing process to a comparable extent (up to 40%). Moreover, we show that there is no clear statistical correlation between gas mixing and typical reservoir characterization parameters such as original gas in place (OGIP), average reservoir permeability, and the Dykstra-Parsons coefficient. Instead, the average time of travel of all reservoir cells calculated from flow diagnostics shows a negative correlation with the level of gas mixing. These results reveal the importance of 3D reservoir architecture analysis (integration of multiple levels of heterogeneity) to UHS site evaluation on gas mixing in depleted gas reservoirs. This study herein provides valuable insights into UHS site evaluation regarding gas mixing.

1. Introduction

The hydrogen strategy pledged by various countries/regions has led to increasing research in Underground Hydrogen Storage (UHS) [1–

8]. Global research efforts have resulted in collection of many fundamental data, such as wettability [9,10], geochemical reactivity in hydrogen-brine-sandstone systems [11], dispersivity [12,13], and relative permeability [14–17]. These experimental findings combined with

E-mail addresses: z.bo@uq.net.au (Z. Bo), kunning.tang@unsw.edu.au (K. Tang).

^{*} Corresponding author at: Gas & Energy Transition Research Centre, University of Queensland, St Lucia, Brisbane, 4072, Queensland, Australia.

^{**} Corresponding author at: School of Minerals and Energy Resources Engineering, The University of New South Wales, Kengsington, Sydney, 2052, New South Wales. Australia.

simulation studies depict a promising future of this large-scale hydrogen storage technology in specific scenarios [18-21]. However, potential obstacles also emerge as the technology is pushed forward toward commercialization. Experimentally measured relative permeability is very low in hydrogen-brine fluid system [14,16,22,23]. Such low hydrogen relative permeability with potential hysteresis during the imbibition process (production period of UHS cyclic operations) may greatly diminish the productivity of this emerging technology [24,25]. Moreover, the requirement that microbial geochemical reactions during UHS operation should be limited and geographic proximity to a potential hydrogen hub [26] may cause some reservoirs with good gas injection/production potential not to be the best choice for UHS [27]. From this perspective, evaluating the feasibility of UHS in porous reservoirs (depleted hydrocarbon reservoirs and saline aquifers) has to be based on criteria from multiple disciplines and compatible with the local hydrogen development strategy [27].

Many studies have been conducted to derive criteria for assessing the feasibility of UHS in porous reservoirs. [28] used Phreegc software to evaluate the static and kinetic hydrogen loss in sandstone environments and found that carbonate-free sandstone reservoirs are favorable for UHS projects. Their findings were proven by experimental observations [11,29]. In terms of potential hydrogen consumption due to microbial growth, [30] conducted a comprehensive literature review of the controls on the three major hydrogen-consuming processes which are methanogenesis, acetogenesis, and sulfate reduction [30,31]. They concluded that temperature and salinity are the most relevant environmental factors to constrain the growth of homoactogens and methanogens and they should be above 55 °C and 1.7 M, respectively. Moreover, numerical simulation using a series of synthetic homogeneous reservoirs indicates that the best permeability x thickness (average reservoir permeability multiplied by formation thickness) should be above $40,000 \text{ mD} \cdot m$ and reservoir dip between $5-10^{\circ}$ from an UHS injectivity/productivity point of view [32]. These criteria are set considering the most important factors that affect the containment or the overall injectivity/productivity of the UHS project, as described by many [33-37]. In depleted gas reservoirs, physical/geochemical/microbial reactions associated with UHS have received considerable research attention [26,38,39] and preliminary criteria have been established. However, geological heterogeneity, as raised by many studies to be the one of the governing factors on UHS storage capacity and gas mixing [34,40,41], has attracted fewer research studies thus far.

Previous studies on the topic of gas mixing during UHS cyclic operations in heterogeneous reservoirs have been summarized in Bo et al. [1], while studies on gas mixing induced by cushion gas behavior have been summarized by Yang et al. [42]. In short, the mechanicaldispersion-induced gas mixing [43,44] between the injected hydrogen gas and the cushion/residual gas in a storage reservoir is affected by various factors such as reservoir dip, target injectivity/productivity, and the components present in the injection gas [45]. Further, Bo et al. [1] use synthetic braided-fluvial depleted gas reservoir models to extend our understanding of gas mixing during UHS into heterogeneous geological settings. Their simulations indicate that the heterogeneous braided-fluvial facies will enhance hydrogen plume spreading (in the gas phase, penetrating the residual methane plume) and degrade the hydrogen fraction in the produced stream compared to a homogeneous case. More than 15% of the recovery is affected over a project life of ten yearly cycles (ten years). In addition, reservoir formation structure is found to dominate this process as facies heterogeneity (channel dimensions) may only influence gas mixing considerably in specific structures. The synthetic reservoir models in [1] are built based on petrophysical properties from depleted gas reservoirs in the Waarree Sandstone of the Otway Basin Australia which are very suitable for gas storage (average porosity above 0.2 with more than 500 mD average permeability) [46]. However, one cannot always expect to get such promising subsurface resources when implementing UHS globally.

Australia can be an example. According to the Australian Renewable Energy Agency, most hydrogen projects in Australia are located along the coastline except a few in the Canning Basin of Western Australia and the Surat/Bowen basins in Queensland [27]. Combined with the geographic availability of depleted gas reservoirs in Eastern Australia [47,48], depleted gas reservoirs in the Surat/Bowen Basin turn out to be one of the best options to be integrated into hydrogen hubs for potential UHS in Queensland and New South Wales. However, the gas storage potential of depleted gas reservoirs in the basin is far from ideal. Based on the history of those gas reservoirs, the single well productivity in the Surat/Bowen Basin is much lower than that of the Otway Basin, and can be explained by poorer petrophysical properties [49]. Furthermore, some of the best depleted gas reservoirs such as the Silver Spring have been used for underground gas storage (UGS) [50].

In a previous study [1], we investigated the role of reservoir scale geological heterogeneity on gas mixing and its result on the composition of the production stream over time in the context of reservoirs that originated from a high-permeability braided-fluvial depositional setting. While previous studies in oil and gas recovery have shown that km-scale and cm-scale heterogeneities are more significant than metrescale heterogeneity in meandering-fluvial systems [51], the unique multi-physics nature of UHS operations warrants a fresh investigation of these effects. This is particularly relevant in meandering-fluvial settings where, due to low depositional fluvial energy, a diverse range of both lithological and property facies exist [52]. The corresponding impact of metre-scale heterogeneity in meandering-fluvial systems on injectivity and productivity during UHS cyclic operations remains largely unstudied.

To facilitate the development of UHS site evaluation criteria on gas mixing, here we further investigate storage reservoirs in sediments accumulated in meandering-fluvial system settings which are more complex in terms of geological heterogeneity than the braided-fluvial system. As in the previous study, the UHS project is assumed to use a depleted gas field. Realistic synthetic reservoir models are built to simulate and gain understanding of the gas mixing processes during UHS operations in such reservoirs. Specifically, the process-mimicking meandering system modeling software FLUMY is used to build static facies models with different geological characteristics such as channel dimensions. FLUMY forward models, i.e. mimics, the dynamics and sedimentation processes in meandering fluvial systems. After incorporating actual petrophysical data from meandering fluvial system reservoirs into an upscaled facies model, numerical simulations can be performed to explore the effects of different levels of heterogeneity on gas mixing during a hydrogen-methane mixture cyclic storage operation. Simulations indicate that channel dimensions and metrescale heterogeneity (10 to 100 m) such as the presence of abandoned channel facies affect the gas mixing processes considerably. Channel dimensions effectively alter the correlation lengths (ultimately the 3D flow path length) of the system, and the presence of abandoned channel facies may cause similar influence on gas mixing depending on its architectural relationships with the meander belt. Statistical analysis on potential impacts from the original gas in place (OGIP) of the gas reservoir and injectivity/productivity in the modeled system are also presented. A new UHS gas mixing evaluation criterion based on reservoir 3D architectures is then proposed accordingly.

2. Methodology

In this section, we first provide a brief review of the origin of meandering fluvial system reservoirs, their reservoir architecture, and the status quo of how they are modeled. A methodology to build stochastic synthetic meandering-fluvial reservoir models is introduced. Finally, simulation cases designed for investigating gas mixing during hydrogen-methane mixture UHS operations in reservoirs originated in meandering-fluvial systems are presented.

2.1. Meandering-fluvial reservoirs in the oil and gas industry

Meandering rivers typically occur in the lower reach of a river's drainage system, where paleoslope is fairly flat. Therefore, the transportational and depositional energy is lower in a meandering-fluvial system compared to a braided fluvial system, such that more finergrained sediments are accumulated with fining-up trend during each sediment cycle [53]. The longitudinal dispersion of the flow velocity due to energy loss at the edge of channels causes erosion on the outside of a river bend, named the cutbank side [53,54]. As the cutbank side loses sediments, the inside river bend, named point bar side, gains sediments and brings about transverse flow toward the cutbank side until the sediment bedform slope is big enough to balance erosion [55]. Depending on the overbank grain sizes, flow energy, and sinuosity of river bends various meandering river geometries form [54]. Moreover, avulsion with different rates and styles (river flow diversion due to river breaking through the overbank after heavy erosion) will lead to the formation of crevasse splays [56] and abandoned channels [52]. With these geomorphological and post-sedimentary processes, one can expect the architecture of a meandering-fluvial system reservoir to be much more complex than that of a braided-fluvial system, thus requiring multiple hierarchical levels to describe the sedimentary system

Meandering-fluvial reservoirs are classified into two categories: reservoirs with incised-valley-fill and meandering-river floodplain deposits, respectively [53]. In this study, we focus on the latter described as channel-and-bar type [57] or meander-belt reservoirs [58]. This type of oil and gas reservoir is characterized by the small size of individual reservoir bodies compartmentalized by fine-grained overbank sediments [59], resulting in hundreds to thousands of individual reservoir units. Thus, the development of these hydrocarbon fields may be extremely difficult [57] and has attracted much modeling and simulation research since the last century.

Researchers [57] use 4 hierarchical levels [51] to describe the internal architecture of a meandering belt structure when investigating the connectivity and potential (oil or gas) recovery of these reservoirs. From small to large scale heterogeneity, levels 1 to 4 control the petrophysical properties (permeability, porosity, and relative permeability), sub-channel structure (channel lag, abandoned channel, and finingupward packages), channel dimension, and meandering belt structure (sand-to-gross ratio and stacking of belts) [51,60]. None of the commonly used geomodelling techniques can exhaustively represent these four levels of heterogeneity and the modeling capabilities with workflows that integrate multiple techniques are still being improved [61, 62]. Because of this, many simulation studies simplify their models when investigating meandering system reservoirs [60]. Simulation for oil recovery predictions is an example where sub-channel structure (level 2) is often overlooked [63,64]. This level of heterogeneity was proven to be less important for oil and gas production compared to the other 3 levels through experimental simulation studies [51]. Similar works have been also done for the same purpose for CO₂ storage [65].

In summary, from its origin, the meandering-fluvial system reservoirs are inherently heterogeneous and pose difficulties for comprehensive reservoir modeling. Thus, specially designed simulation studies are needed to reveal the relevant levels (scales) of heterogeneity to be modeled in UHS projects.

2.2. Meandering-fluvial system facies modeling with FLUMY

This study aims to investigate the effects of multiple levels of heterogeneity on mechanical dispersion-induced gas mixing during UHS in meandering-fluvial system reservoirs. Traditional geomodeling methods such as object-based modeling, sequential indicator simulation, or multipoint statistics may not be suitable for building the facies model here. This is because they have difficulty in capturing either the vertical or horizontal architectural relationships between point bar

Table 1
Facies code for 3-facies and 4-facies models simplified from the FLUMY 9-facies model.

3-facies	4-facies	
1 (Channel)	1 (Channel)	
2 (Point bar)	2 (Point bar)	
3 (Background)	3 (Background)	
-	4 (Abandoned channel)	
	1 (Channel) 2 (Point bar)	

facies and various channel facies [62]. Instead, a process-mimicking simulator (FLUMY) is used for building a model of the complex spatial distribution of multiple facies in the meandering-fluvial system [62,64].

In FLUMY, given constant paleo-slope and erodibility coefficient (assuming the same sedimentary environment), different reservoir architectures can be generated via varying channel dimensions and avulsion [66]. FLUMY uses a static model with nine facies to represent different meandering-fluvial reservoir architectures A. In this simulation study, several facies have similar hydraulic conductivity, therefore they are not necessary. Thus, a 3-facies model is built to focus on the placement of accretion packages and channel geometries. Further, to incorporate level 2 heterogeneity, the mud plug facies in the abandoned channel is separated from channel facies to build a 4-facies model. Table 1 shows the facies classification codes of two models. We simulate two channel dimensions (see Table 2) in FLUMY for both 3-facies and 4-facies models.

The channel dimensions input into the FLUMY simulation are based on reservoir analogues and meandering fluvial databases. River channel depths in meandering systems are found statistically to be less than those in braided-fluvial systems, most of which range from 4 to 10 m [67,68]. Based on this, channel depths of 5 m and 10 m are selected from analogues such as the Daqing oil field in China (6 m sand thickness) [69], Moonie oil field in Australia (3 to 20 m sand thickness) [70], and Kern River fields in U.S. (2 to 15 m sand thickness) [71]. The channel width-to-depth ratio is set to 10 according to the most common range [68]. Other parameters including avulsion, aggradation, and erodibility coefficient are set such that analogous sheet-type point bars (fixed sand-to-gross ratio of 50%) will be generated from the two channel sizes. Table 2 provides all the essential input parameters for FLUMY to generate meandering-fluvial facies models in a reservoir domain consisting of 92,480 grid cells ($68 \times 68 \times 20$) 1,005 m long and wide, and 20 m thick. For each channel size, 5 facies models are generated while all are conditioned to well facies data (the well is located in the center of the model) from the Evergreen formation in the Surat Basin, Australia which is well characterized as a distributary channel system [70]. Trial and error runs with manual checks are performed after each facies model simulation to make sure the lithofacies well data are honored. It is noteworthy that the depositional setting with different channel size cases and different static model realizations is not primarily intended to study the effects of channel sizes or realizations on reservoir responses. Rather, this setting provides diverse geological contexts in which to examine how abandoned channel facies (presented in the 4-facies models) affect flow behavior under different architectural conditions. This approach allows us to systematically investigate the impact of metre-scale heterogeneity across a range of realistic meandering fluvial architectures (having enough realizations to present the possibly diverse results).

This resulting synthetic facies distribution reservoir model is set as normally pressurized (15,030 kPa at gas-water contact at a depth 1506 m) with a temperature gradient (30.4 °C/km) and a zero regional dip. The synthetic reservoir is assumed to host a gas field with noflow boundaries for the gas phase (shale with high threshold capillary pressure for gas) with aquifer support (volume of $68.1*10^5$ m³).

Table 2
Parameters set used in FLUMY to generate the facies models.

Parameter	Small channel	Large channel
Channel depth (m)	5	10
Channel width (m)	50	100
Channel wavelength (m)	625	1250
Regional avulsion (year)	Poisson type = 800	Poisson type = 800
Erodibility coefficient (-)	5.1×10^{-8}	7.3×10^{-8}
Aggradation thickness (m)	0.167	0.333
Domain dimension (m)	$1005 \times 1005 \times 20$	$1005 \times 1005 \times 20$
Grid size (m)	15 × 15	$15 \times 15 \times 1$
Number of realizations generated (-)	5	5

Table 3Variogram parameters for populating the porosity values.

Parameter	Flow-unit	Non-flow-unit
Nugget	0.01	0.01
Type	Spherical	Spherical
Ranges (major, minor, vertical, m)	1000, 500, 10	750,750,7
Angles (major, minor, vertical, °)	90, 0, 0 (channel direction)	0, 0, 0
Average porosity	0.16	0.06
Standard deviation	0.025	0.020

2.3. Property modeling

Before being transformed into dynamic models, 4-facies and 3-facies models are upscaled (volumetrically upscaled into grid size of $30\times30\times1$ m) and further simplified into a model which only consists of flow and non-flow facies. Background (code 3 in Table 1) and abandoned channel (code 4 in Table 1) facies are lumped into non-flow-units, while the point bar (code 2 in Table 1) and channel (code 1 in Table 1) facies are lumped into flow-units. Sequential Gaussian Simulation is used to populate porosity based on these flow-unit models with 10 fixed simulation seeds for building 10 stochastic realizations of each facies model (50 realizations in total for each simulation case). We use a revised Kozeny-Carman equation to calculate the permeability based on porosity (Eq. (1)).

$$k = \frac{1}{180} \frac{\phi^3}{(1 - \phi)^2} d_{K-C},\tag{1}$$

where ϕ is the porosity and d_{K-C} is a function of pore diameter and rock facies set as 3×10^6 . Based on the criteria presented in [32], the permeability thickness of a reservoir should at least range between 1000 to 10,000 mDm to be considered as a UHS candidate. Accordingly, the porosity and permeability of these synthetic reservoirs would range from 0.1 to 0.2 and 50 to 500 mD (calculated from the permeability thickness criteria in [32]), respectively [70,71]. Such ranges are consistent with many meandering-fluvial system reservoirs, such as Rocky Ridge field in North Dakota U.S. [72], Coyote Creek field in Wyoming U.S. [59], and Richmond field in Bowen Basin Australia [49]. Therefore, for the flow-unit facies, sandstone petrophysical data from the Rocky Ridge field [72] are used. Published experimental data from the Bakken shale are used for non-flow-unit (see Table 3). Fig. 1 shows areal views of 3-facies models of small and large channel sizes together with their corresponding permeability distribution. There is good agreement between facies models and upscaled permeability models.

Capillary pressure and relative permeability data (air-brine system, including imbibition) are available from core samples from the Waarree sandstone in the Otway Basin of Australia [46]. The same relative permeability models as those in a previous study [1] are used. The reason for this is twofold. One is given the significant effects of relative permeability on the injectivity/productivity of UHS projects [24], using the same relative permeability to the previous study helps comparison with the geological heterogeneity-induced gas mixing of that previous study. The second reason is that the stored gas in this study is a hydrogen-methane mixture with only 10 mol% hydrogen. We then

assume the methane relative permeability acts as a proxy for the flow behavior of the hydrogen-methane mixture in the reservoir [1,23]. Capillary heterogeneity is considered through a Leverett J function which is routinely used [73,74]. Finally, capillary pressure hysteresis is not considered in this study as the scale of reservoir simulation is much larger than the characteristic capillary dimension [75] and related experimental hysteresis capillary pressure data are not available [46].

2.4. Simulation setup

This study uses a similar simulation schedule to the studies [1,24]. The commercial compositional simulator CMG-GEM is used to model multi-phase fluid flow in porous media and calculates the fluid properties (density, viscosity, phase, compressibility) with a Peng-Robinson cubic equation of state [48]. Appendix B presents a detailed description of the governing equations used in this study to model the mixing between hydrogen and methane. Regarding the well and simulation schedule setup, a single vertical injection/production well is placed in the center of the model. The well schedule consists of three stages, (1) primary production of methane from the reservoir, (2) initial injection using a hydrogen-methane mixture with 10 mol% hydrogen, followed by (3) 10 cyclic operations with the same hydrogen-methane mixture as injection gas. The period of each cycle is 1 year and an injection/production scheme of '6 month-6 month' as described in [1] is used in all cases. In the '6 month-6 month' scheme, a hydrogen-methane mixture is injected for six consecutive months and then produced for the next six months and this is repeated for 10 years (10 cycles).

The simulation schedule and injection/production rate are set based on production history from the depleted meandering-fluvial gas reservoirs in the Surat/Bowen Basin which have similar petrophysical properties (injection/production rate ranges from 0.12 * 10⁶ m³/day to 0.6 * 10⁶ m³/day) [49]. These injection and production periods are longer than those used in other UHS reservoir simulation studies [44,45,76]. These longer periods are selected for this study in order to better compare and contrast the cases. All cases are subjected to the same pressure constraints at the wells. The maximum bottom hole pressure for the injection well is set to 15,000 kPa to ensure that reservoir pressure does not exceed the initial reservoir pressure, and the minimum bottom hole pressure for the production well is set to 5000 kPa to maintain the minimum pressure required for transportation and processing downstream [73]. Table 4 shows the detailed simulation setup of each case. As hydrogen-methane mixture is injected, it displaces and mixes with the existing gas in the reservoir. When the gas mixture is subsequently produced it experiences changes in composition as the injected hydrogen has been diluted by mixing with residual/cushion gas. In each injection-production cycle, the hydrogen fraction in the produced gas is changing but over time it is expected to come closer to the initial injection composition. The reservoir heterogeneity caused by how different sediments are distributed spatially affects how the gases mix and imposes an uncertainty on the produced gas composition.

3. Results and discussion

The simulation results are used to show the effects of channel size and presence of abandoned channels on the distribution of hydrogen in subsurface and the composition of the production stream, i.e. the fraction of hydrogen in the produced methane/hydrogen mixture. Each case comprises 50 realizations that allow uncertainty to be explored. Uncertainty is expressed as the difference between the P10 and P90 realizations. Finally, flow diagnostics on the realizations is employed to explore if our proposed dimensionless group numbers can help to characterize gas mixing in UHS as it is practiced in the oil and gas industry.

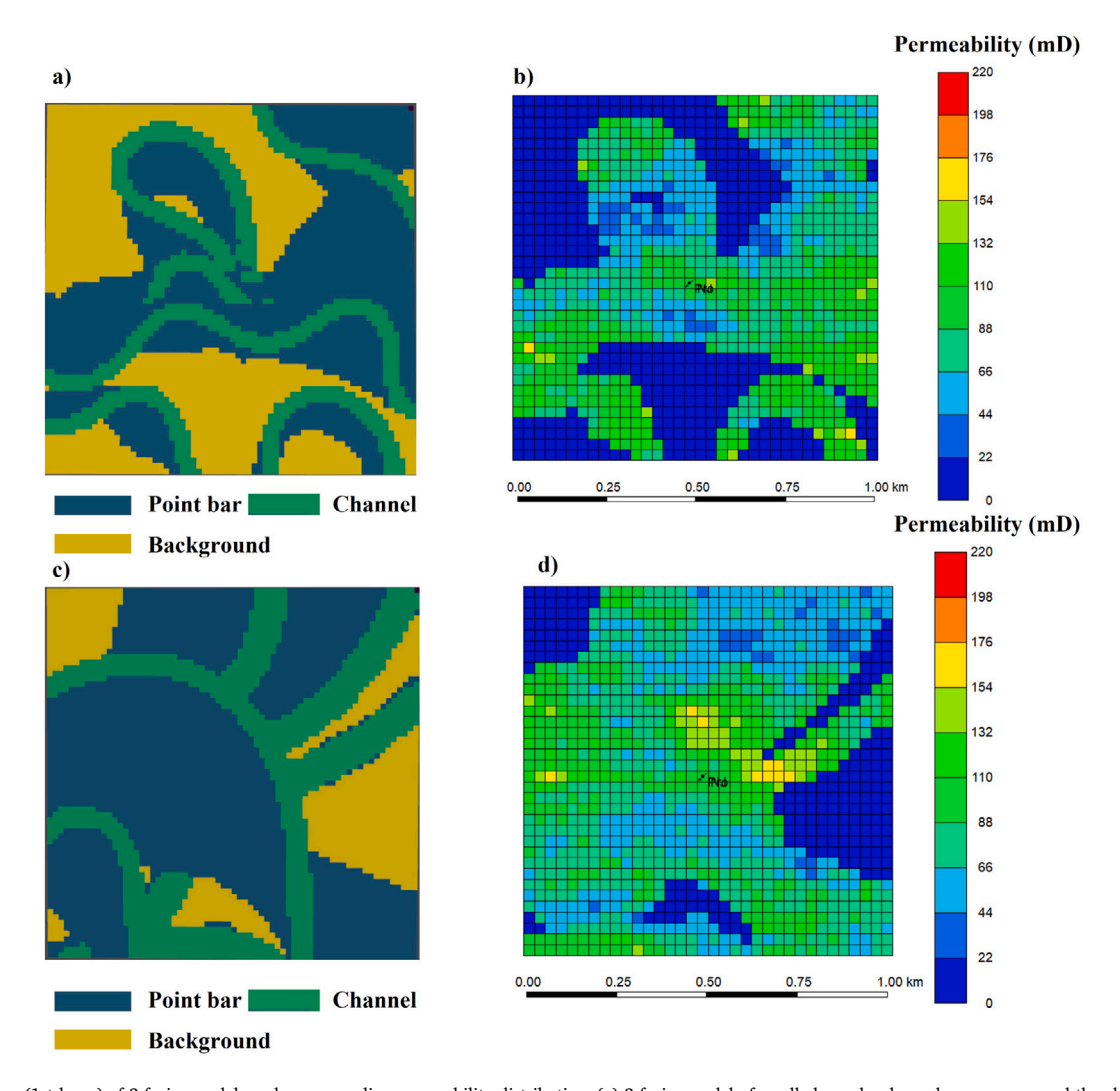


Fig. 1. Areal views (1st layer) of 3-facies models and corresponding permeability distribution; (a) 3-facies model of small channels, channels are narrow and the channel wavelength is small and associated point bars; (b) Permeability distribution of (a), flow units form tortuous flow paths from injection/production well in the center of the reservoir; (c) 3-facies model of large channels, channels are wider than that of (a) with larger channel wavelength and associated point bars; (d) Permeability distribution of (c), flow units are widely spread over the reservoir with a regular channel belt geometry.

Table 4Overview of the simulation setup for each case.

Case No.	Channel dimension	Facies model	Inj/Pro rate (* 10 ⁶ m ³ /day)	Inj/Pro scheme	Total realizations
1	Small	3-facies	0.35	6 month-6 month	50
2	Small	4-facies	0.35	6 month-6 month	50
3	Large	3-facies	0.35	6 month-6 month	50
4	Large	4-facies	0.35	6 month-6 month	50

3.1. Effects of channel sizes

Hydrogen fraction plumes (spatial distribution of injected hydrogen) show distinct geometries when injected in geological settings with small and large channels, respectively, resulting in a different uncertainty (P10 and P90 realization difference) of the hydrogen fraction in the produced stream. Fig. 2 provides areal views (1st layer) of the hydrogen fraction plumes from two realizations of cases 1 and 3 by the end of the 10th cycle. In both small and large channels, the hydrogen fraction is greater in non-flow units (blue regions in Fig. 2). This is because the flow and spreading-induced gas mixing of the hydrogenmethane mixture is limited in non-flow units due to low permeability

(1 to 4 mD, allows limited gas flow and mixing). In contrast, such hydrogen-methane mixture displacement (spreading) is more efficient in flow units, resulting in a higher methane fraction during each production period. Thus, the hydrogen plume in case 1 (Fig. 2 a) shows an irregular discontinuous pattern interbedded with narrow flow paths (flow units) originating from small channel sands. The hydrogen fraction plume in case 3 (Fig. 2 b) is more locally-centralized and continuous in shape.

The variation in hydrogen fraction plume geometry leads to uncertainty (P10 and P90 realization difference) in the hydrogen fraction in the produced stream. The profile of hydrogen fraction (composition through time or after each cycle) in the produced stream of all cases

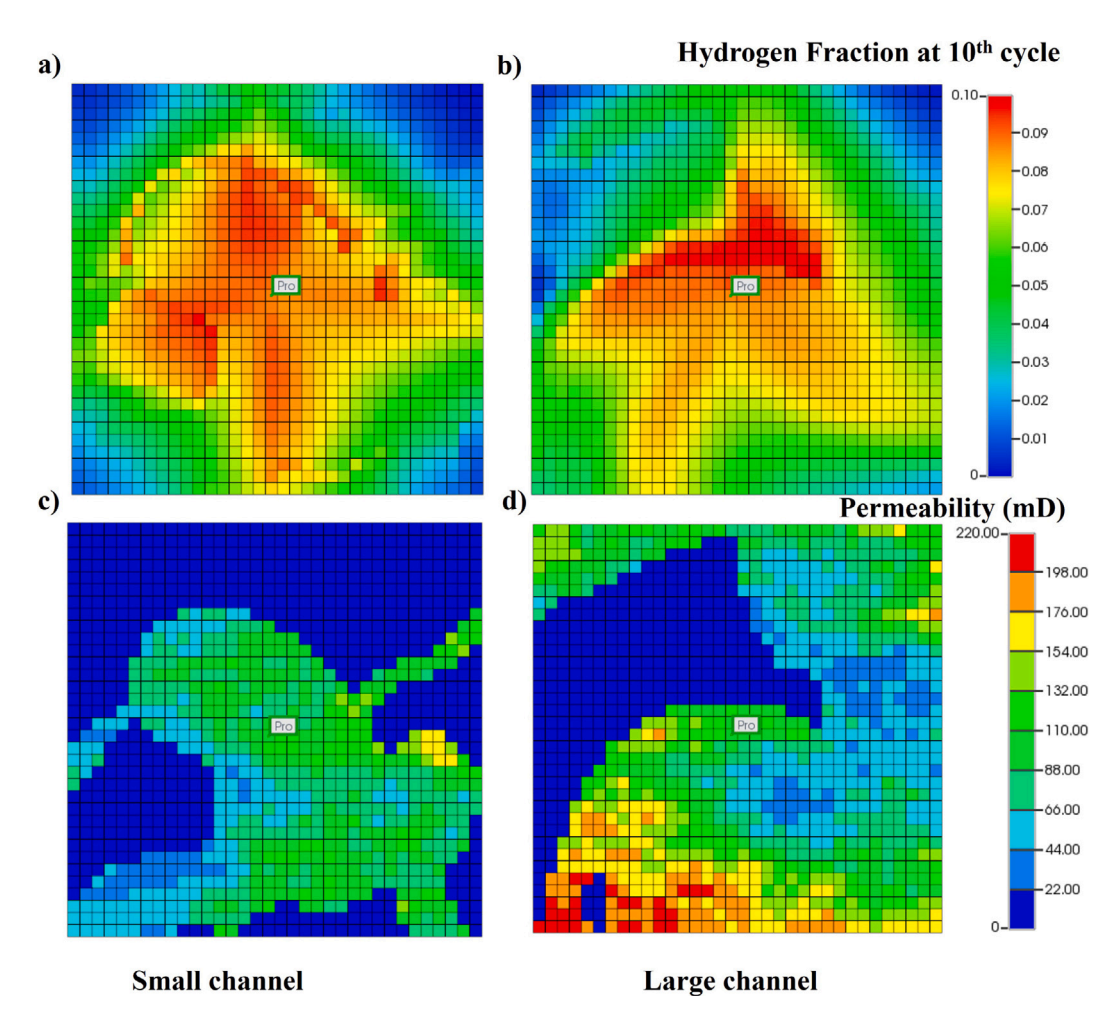


Fig. 2. Examples of areal view (1st layer) of (a) Hydrogen fraction plume by the end of the 10th cycle from the small channel (case 1) and (b) Large channel (case 3); hydrogen is bypassed by hydrogen-methane mixture displacement front flowing towards the production well, resulting in hydrogen concentrated in low permeability areas or non-flow-units; while these high-hydrogen regions are interbedded with narrow flow paths in small channels (case 1), large channel cases (case 3) show more continuous and locally-centralized hydrogen fraction plumes; (c) Permeability map of the small channel (case 1); (d) Permeability map of the large channel. (For interpretation of the references to color in this figure legend, the reader is referred to the web version of this article.)

shows a similar decreasing trend during each production period as observed in our previous studies [1]. To examine the uncertainty of hydrogen fraction out of 100 realizations in cases 1 and 3, the cumulative number of days in which the hydrogen fraction drops below 0.09 (90% of injected hydrogen fraction) is computed. Fig. 3 shows the P50, P10, and P90 of cumulative days of hydrogen fraction in produced stream below 0.09 from the 50 realizations of case 1 (Fig. 3 a) and case 3 (Fig. 3 b). The P50 of cases 1 and 3 are comparable as they differ by only 1.9%. The P90 differs by 6%. However, the P10 differences for case 1 (543 days) is 17.1% less than that of case 3 (636 days). The uncertainty range (difference between P10 and P90) of the hydrogen fraction in the produced stream is displayed by the length of the black error bar on the graph and that of case 1 is 42.4% less than that of case 3

The smaller gas mixing uncertainty of the small channel case (case 1) originates from the tortuous geometry of flow-units in the facies models (see Fig. 1). In this study, the only driving mechanisms considered are gravity, capillary, and viscous forces, respectively. The hydrogen concentration of a grid block in the model is thus a hyperbolic function of the volume of fluids flowed into and out of the grid block (direction-dependent, relative to the production/injection well). The torturous nature of these flow units in the small channel case creates more constrained flow paths, resulting in a more restricted spreading area of the stored hydrogen-methane mixture compared to the large channel case. In contrast, the large channel case (case 3) features a

less restricted sweep area and longer correlation length of the system, which distributes stored fluid flows across more grid blocks. Such a broader spreading area increases the contact area between the stored hydrogen-methane mixture and the connate pure methane, intensifying gas mixing and leading to a larger uncertainty in produced gas stream composition [1,77], as shown in Fig. 3 (b). Here the meandering-fluvial system facies modeling workflow, the difference between the small and large channel cases is primarily illustrated through the generated meander belt geometries, instead of the specific geometry of individual channels. In practice, such information on flow-unit geometry will be available from the isopach of any depleted gas reservoirs [57]. Analysis and conclusions here will facilitate the assessment of potential gas mixing in UHS projects.

3.2. Effects of abandoned channels

The presence of abandoned channels in meandering-fluvial systems will affect the gas mixing processes during UHS differently, depending on their location and architectural relationship with the meander belts. The extent of this effect is comparable to that of channel sizes in certain cases. Fig. 4 shows the cumulative days of hydrogen fraction below 0.09 from the simulation performed on 100 realizations of cases 2 and 4. While their P50s are similar (P50 of case 4 is 4.6% smaller than case 2), the uncertainty of the two cases are also comparable (6.8% difference). Compared to the results from Fig. 3, abandoned channels intensify gas

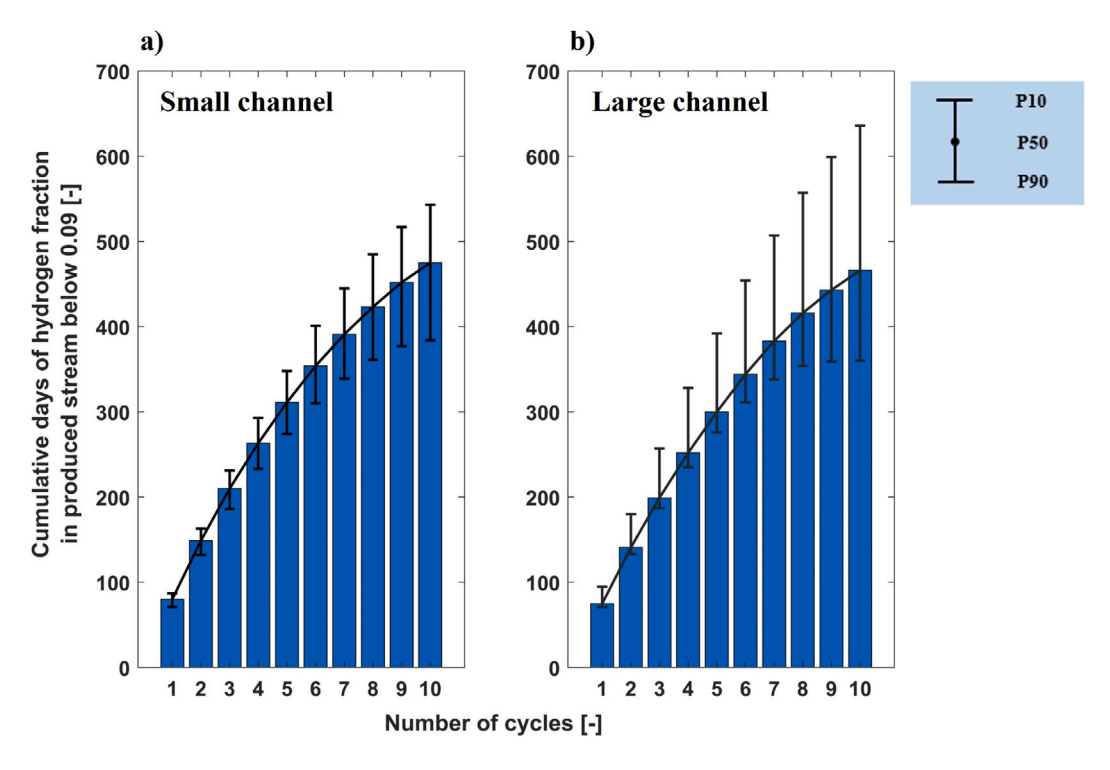


Fig. 3. Bar graphs showing the P50 of cumulative days of hydrogen fraction in produced stream that drop below 0.09 in 50 realizations from (a) case 1 (small channel); (b) case 3 (large channel) with error bars marking the corresponding P10 and P90; The length of the error bar gives an idea on the magnitude of uncertainty.

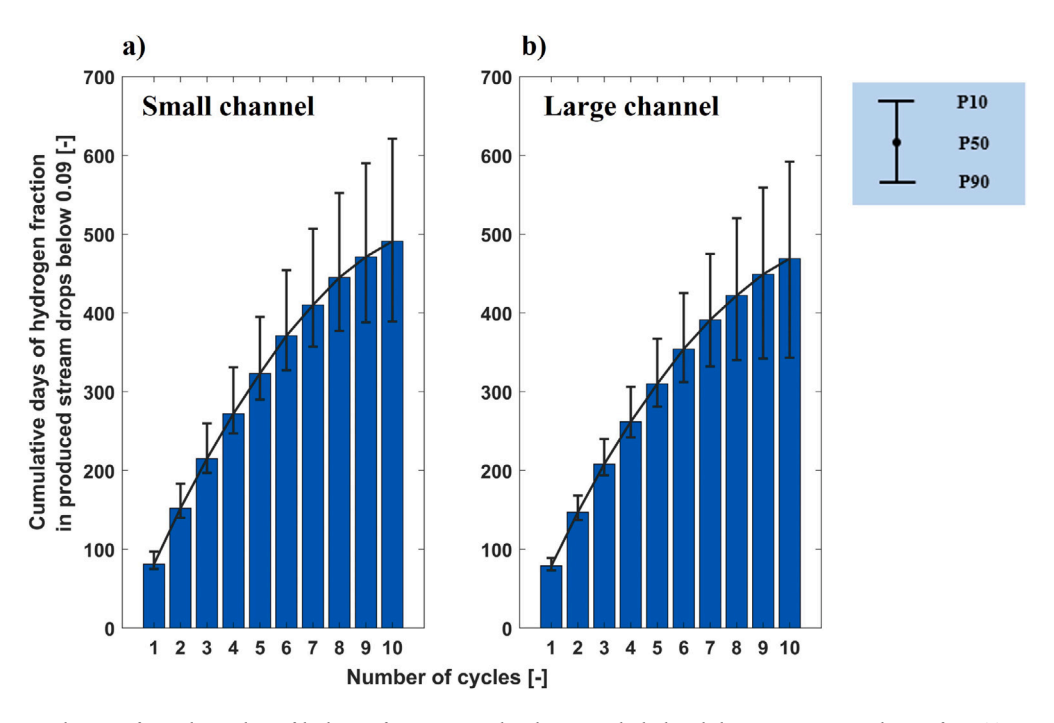


Fig. 4. Bar graphs showing the P50 of cumulative days of hydrogen fraction in produced stream which drop below 0.09 in 50 simulations from (a) case 2 (small channel with abandoned channels from 4-facies models); (b) case 4 (large channel with abandoned channels from 4-facies models) with error bars marking the corresponding P10 and P90.

mixing and degrade the hydrogen fraction in produced streams in the small channel case. They retard gas mixing and improve the hydrogen fraction in the produced stream of the large channel case. To further understand such opposite roles played by the abandoned channel in the small and large channel cases, we analyze and compare the reservoir architectures of each facies realization together with the corresponding production profile.

Abandoned channels in reservoir realizations of case 2 tend to appear in the middle of meander belts, partially blocking the connections

between point bar facies units and trapping more hydrogen gas. Fig. 5 (a) and (b) shows point bar facies in case 2 are disconnected from each other in the middle by abandoned channels. The resulting P50 of 10 realizations cumulative days hydrogen fraction below 0.09 increases by 15% and 14%, respectively. This originates from the formation of abandoned channel facies which inherit the geometry of the active channels and deposit at the upper part of the fining-upward packages [52]. Thus, when the abandoned channel facies deposit forms borders between point bar facies units, they may act as barriers or baffles (non-flow

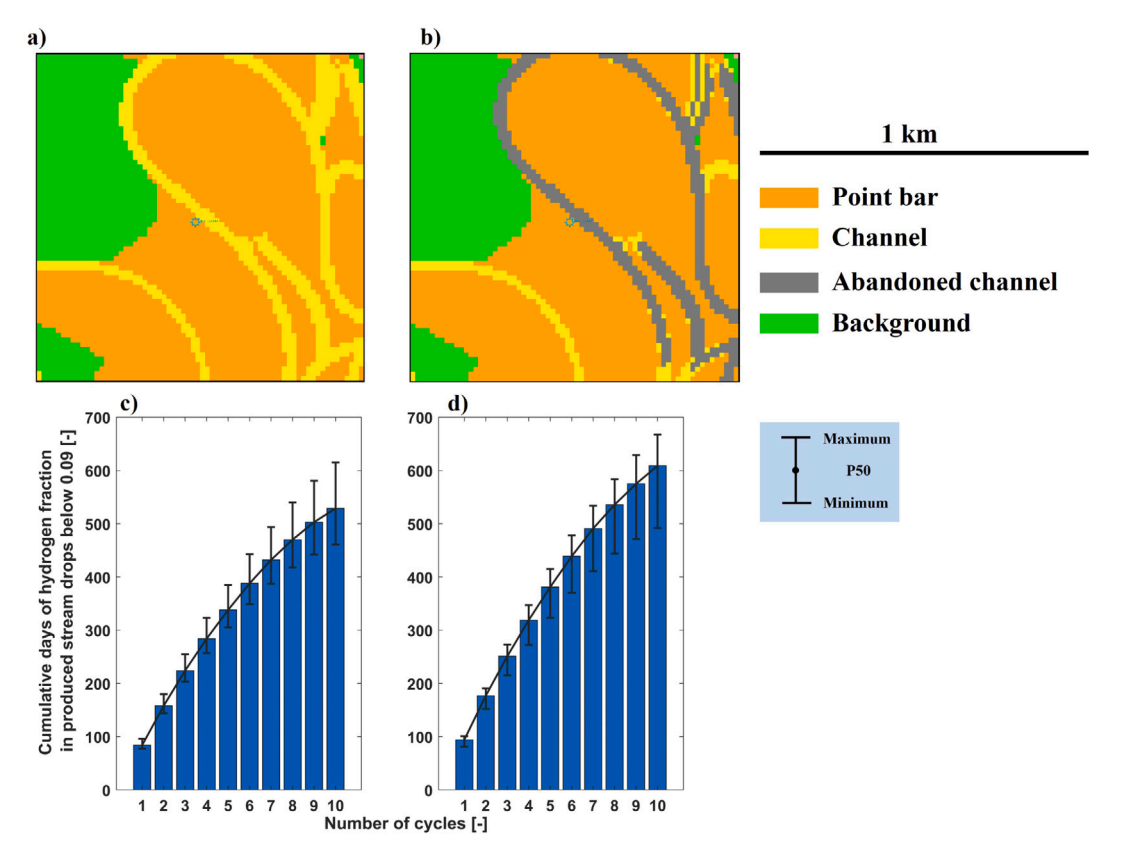


Fig. 5. The areal view of one realization in (a) case 1, 3-facies model; (b) case 2, 4-facies model, showing abandoned channels blocking connections between point bar facies, and their corresponding maximum, minimum, and P50 of cumulative days hydrogen fraction in produced stream below 0.09 from 10 realizations. (c) case 1; (d) case 2.

units) to hydrocarbon flow in oil and gas fields [58]. During UHS injection periods, the channel lag facies (located vertically beneath the abandoned channel facies) allow the hydrogen-methane mixture to flow into the adjacent point bar across the abandoned channel facies. With the same injected volume of gas, these abandoned channel facies significantly alter and lengthen the flow paths. In Case 1, where abandoned channel facies are absent, the hydrogen-methane mixture flows directly through adjacent point bar units. However, in Case 2, the presence of abandoned channel facies forces the injected fluid to flow through more tortuous paths. The gas mixture must flow both above (through overlying point bar deposits) and beneath (through underlying channel lag facies) the abandoned channel barriers to reach adjacent point bar units. This three-dimensional flow diversion around the impermeable abandoned channel facies considerably lengthens the flow path. Such prolonged flow paths intensify gas mixing via a larger mixture spreading area [77] and result in a decrease in hydrogen fraction in produced streams shown in Fig. 5 (c) and (d).

The presence of abandoned channels in case 4 occurs commonly at the fringe of the meander belt instead of within it which decreases the correlation length (ultimately flow path length) of the system and retards gas mixing. Because of the difference in channel wavelength of small and large channels, the channel facies in large channels tends to deposit rarely in the middle of the meander belt. Consequently, as shown in Fig. 6 (a) and (b), these abandoned channel facies will block the connection between point bar facies inside the channel belt and other units outside it (either a non-flow background or a flow-unit facies). Under this circumstance, the correlation length of the system reduces, resulting in a significant flow path and uncertainty range decrease (40%) in Fig. 6. Such influence is comparable to that from channel sizes between cases 1 and 3. It is noteworthy that, the workflow for generating facies models in this study is designed to keep a constant sand-to-gross ratio across cases, thus the channel wavelengths of small and large channels are set to be distinctive. Therefore, the results and

interpretation presented here are intended to demonstrate the potential effects of abandoned channels with described spatial distributions (such as those in Figs. 5 and 6) on UHS gas mixing. It is important to note that these findings do not suggest the potential spatial distribution of abandoned channels in actual meandering-fluvial reservoirs with small and large channel sizes. Instead of facies modeling, the correct prediction of the spatial distribution of abandoned channels in a meandering-fluvial reservoir should be based on further research on the target reservoir region.

3.3. Characterization of UHS gas mixing

UHS in a depleted gas reservoir with residual methane (natural gas) as the cushion gas is a miscible displacement process in the gas phase [1]. Previous studies characterize such a miscible displacement process in heterogenous porous reservoirs with several dimensionless group numbers (scaling analysis) such as the Péclet number, mobility ratio, the Dykstra-Parsons Coefficient (V_{DP}) , and dimensionless correlation length [1,77,78]. Under a same scaling group, flow systems in heterogeneous media will show roughly the same level of gas mixing [77]. These dimensionless group numbers work well in 2D reservoir models [77,78]. Problems arise when characterizing the reservoir with complex spatial 3D architecture. For example, when using dimensionless correlation length in 2D as an index for the potential flow path in the realizations shown in Fig. 5, the correlation length of case 1 will be greater (instead of less in terms of the 3D flow path in reality) than that of case 2 due to the abandoned channel. Thus, 3D characteristics such as a local connected sand body (local connectivity) [64] are used to estimate the performance of this type of reservoir. However, to the best of our knowledge, these characteristics have not been used for characterizing gas mixing during UHS.

To facilitate the future estimation of UHS gas mixing based on reservoir architectures (integration of multiple levels of heterogeneity),

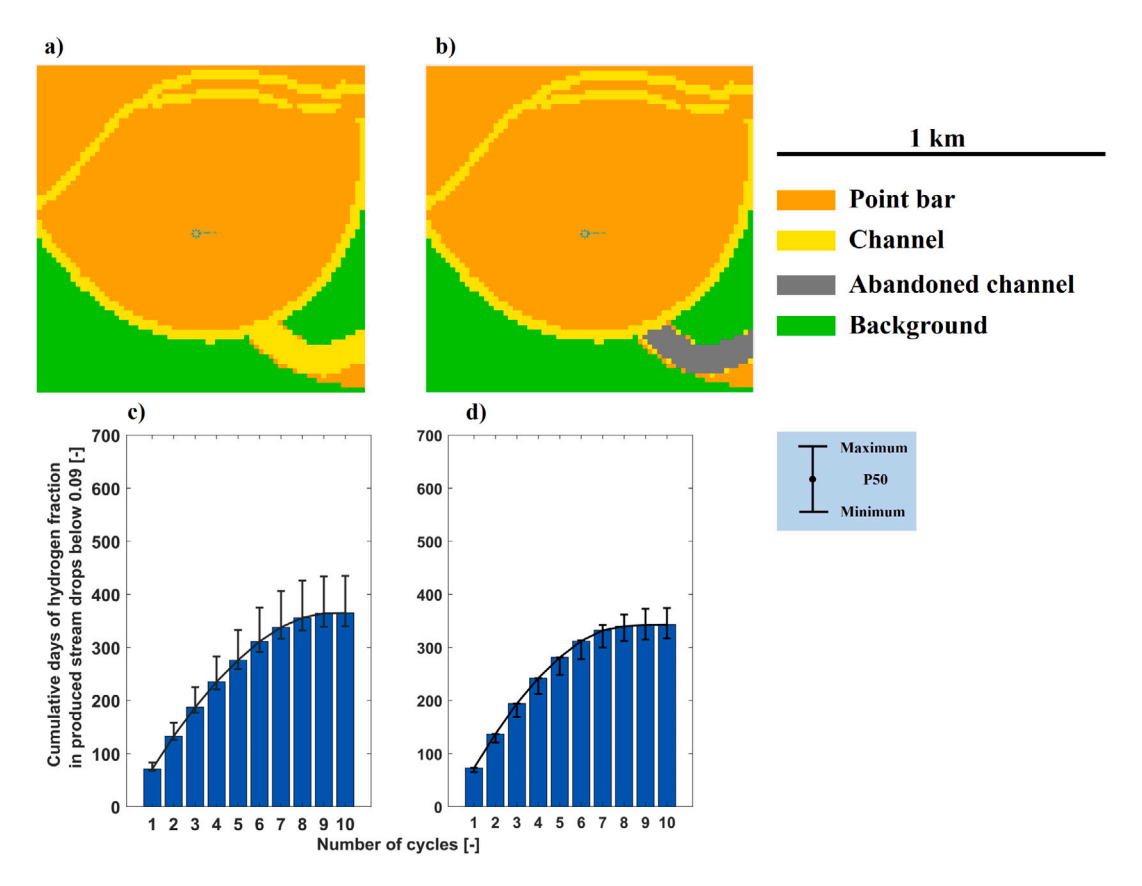


Fig. 6. The areal view of one realization in (a) case 3, 3-facies model; (b) case 4, 4-facies model, showing abandoned channels blocking the only flow path outside the meander belt, and their corresponding maximum, minimum, and P50 of cumulative days hydrogen fraction in produced stream below 0.09 from 10 realizations, (c) case 3; (d) case 4.

we perform flow diagnostics on all the realizations in each case to analyze the correlation between local connectivity and gas mixing (expressed in this study as the cumulative days in which the hydrogen fraction is below specification). Flow diagnostics reveal key flow behavior of reservoir realizations with reduced physics, using a single-phase pressure solution [79]. Typically, the key outputs of flow diagnostics are the local 'time of travel' of each reservoir grid cell from a set of given injection and production wells. In this study, only one production well is used in flow diagnostics which is also located in the center of the reservoir models (same as the numerical simulations). Here, flow diagnostics is performed with the MATLAB reservoir simulation toolbox (MRST) [80]. The total computational time for the 200 realizations in this study is less than a minute, much faster than the conventional full physics numerical simulation. For each reservoir realization, the average time of travel of all reservoir cells is collected and plotted against the cumulative days hydrogen fraction in the produced stream that is below 0.09 to study their correlation.

Fig. 7 shows scatter plots of the cumulative days that hydrogen fraction in the produced stream drops below 0.09 in all reservoir realizations of all 200 reservoir model realizations against the average time of travel of each reservoir cell, Dykstra–Parsons coefficient, average reservoir permeability, and reservoir original gas in place at surface condition. The Dykstra–Parsons coefficient is a commonly used dimensionless group number for characterizing miscible displacement [77]. Meanwhile, reservoir average permeability and original gas in place are good indicators of the total hydrogen mass recovery of UHS project (see Fig. 8). In Fig. 7, gas mixing level is negatively correlated with the average dimensionless time of travel of all reservoir cells while there are no clear correlations with the other three parameters.

Parameters such as permeability and the Dykstra–Parsons coefficient are commonly used as criteria for screening/ranking reservoir realizations or scaling analysis in reservoir management problems [32,

77,81]. The results presented in this study show that these parameters work well as an indicator for estimating UHS injectivity/productivity. However, as discussed previously, gas mixing during UHS operations is a complex process. A meter-scale heterogeneity variation may cause considerable changes in gas mixing level and this variation happens in 3D. Since the afore-mentioned parameters are not designed to describe 3D architectural relationships, there are no clear correlations between gas mixing level and Dykstra–Parsons coefficient, average permeability, and the original gas in place. Our study shows that the average dimensionless time of travel of reservoir cells may act as an indicator for estimating UHS gas mixing but further investigation is needed as their correlation is not strong enough to be diagnostic.

4. Conclusion

In this study, following our previous study [1], we designed a workflow for investigating reservoir and metre-scale heterogeneity effects on UHS gas mixing. The conclusions are summarized below.

- 1. The geometry of a meander belt with various channel dimensions has a significant effect on gas mixing. Meander belts with small channels tend to generate tortuous flow paths interbedded with non-flow units, whereas meander belts with large channels lead to wide and continuous flow paths. These reservoir characteristics result in contrasting gas mixing behaviors where the uncertainty range (difference between P10 and P90) of the hydrogen fraction in the produced stream is 42% more for a large channel case than that of a small channel case.
- 2. Metre-scale heterogeneity (10 to 100 m) such as the presence of abandoned channels results in contrasting effects on gas mixing during UHS depending on their location and architectural relationship with the meander belts. On the one hand, abandoned channels in the middle of the meander belt may act as impermeable units and prolong flow paths during injection periods of cyclic operations: the hydrogen fraction in

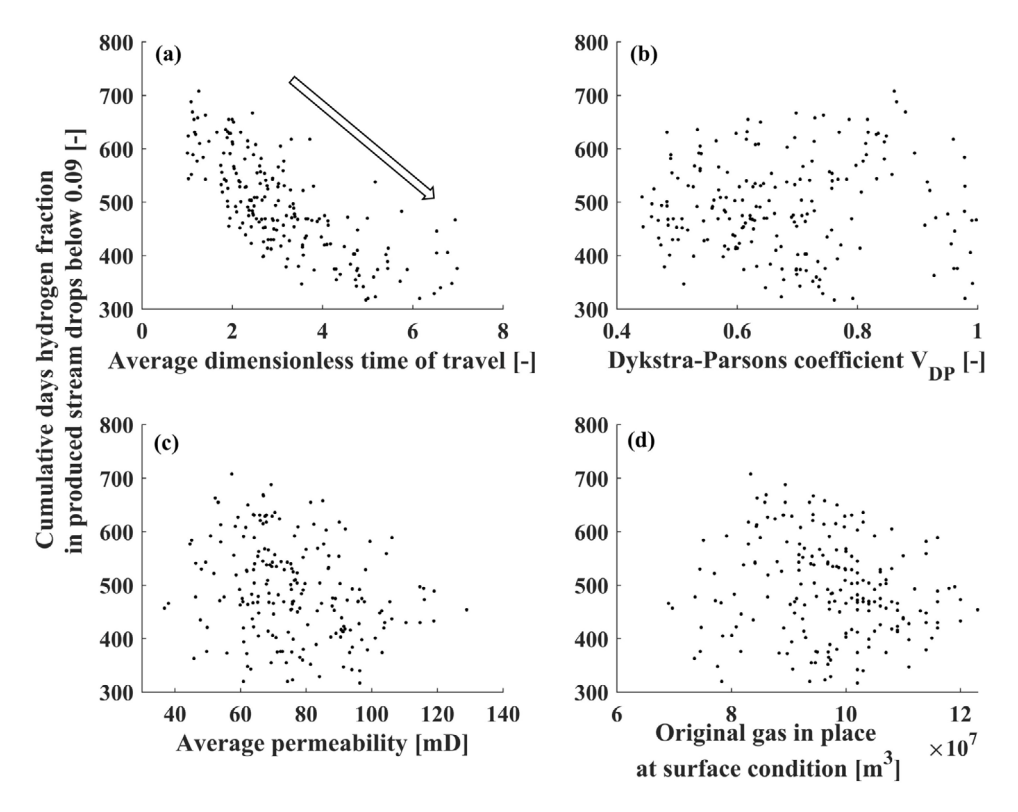


Fig. 7. Scatter plots of the cumulative days hydrogen fraction below 0.09 of all reservoir realizations in each case with (a) the average time of travel of all reservoir cells from flow diagnostics; (b) the Dykstra-Parsons coefficient (V_{DP}) ; (c) the average reservoir permeability; (d) the original gas in place at surface condition.

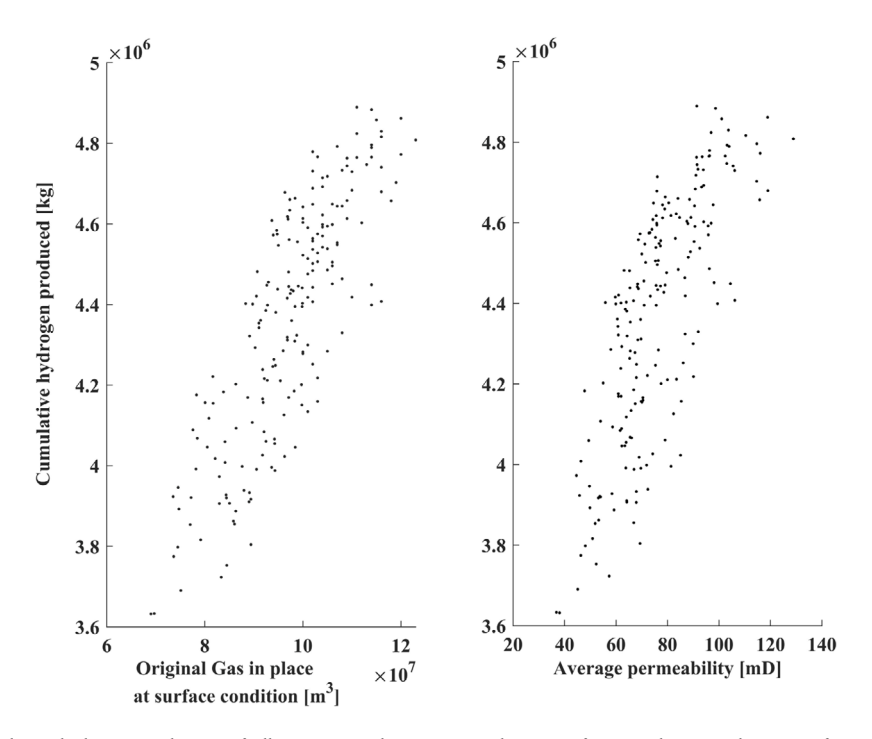


Fig. 8. Scatter plots of the cumulative hydrogen production of all reservoir realizations in each case. Left: original gas in place at surface condition; right: reservoir average permeability.

produced streams is reduced. On the other hand, abandoned channels at the fringe of meander belts may block the connection between the meander belt with other flow units, effectively decreasing the flow path (correlation) length of the system and retarding the gas mixing. Abandoned channels affect the uncertainty range of hydrogen fraction in the produced stream by up to 40%.

3. In meandering-fluvial reservoirs, gas mixing due to mechanical dispersion is governed by 3D reservoir architecture (integration of multiple levels of heterogeneity). Conventional reservoir characteristics such as average permeability, the Dykstra–Parsons coefficient, and original gas in place are not useful UHS gas mixing indicators. More research attention should be paid to new reservoir characterization

methods such as flow diagnostics proposed in this study for rapid characterization of UHS gas mixing.

The results of this study reveal the complex gas mixing behavior of injected gas into meandering-fluvial reservoirs where up to 37% of volumetric recovery is affected. This and our previous study provide valuable insights into UHS site evaluation based on gas mixing and showed the significant difference in gas mixing behavior in reservoirs originated in braided-fluvial versus meandering fluvial settings.

CRediT authorship contribution statement

Zhenkai Bo: Writing – original draft, Software, Methodology, Investigation, Formal analysis, Conceptualization. Sebastian Hörning: Writing – review & editing, Supervision, Software, Formal analysis. Kunning Tang: Writing – review & editing, Software, Investigation, Formal analysis. Jim R. Underschultz: Writing – review & editing, Supervision, Investigation, Formal analysis. Suzanne Hurter: Writing – review & editing, Supervision, Methodology, Investigation, Funding acquisition.

Declaration of competing interest

The authors declare that they have no known competing financial interests or personal relationships that could have appeared to influence the work reported in this paper.

Acknowledgments

This research has been partially funded by the Energi Simulation Industrial Chair program, Australia. Energi Simulation is a not-for-profit organization based in Canada. This research has also been funded by The University of Queensland Gas & Energy Transition Research Centre, Australia and its industry members (Arrow Energy, Australia Pacific LNG and Santos). Zhenkai acknowledges the University of Queensland and Energi Simulation for the University of Queensland Research Training Stipend and Research Higher Degree Top Up Scholarships. We would also like to thank MINES ParisTech for their software FLUMY™, process-based channelized reservoir models. Copyright©MINES PARIS-PSL/ARMINES.

Appendix A. 9-facies model in FLUMY

In FLUMY, the 9-facies model represents different types of sediments in meandering systems by mimicking channel migration during sedimentation. Lateral accretion packages are composed of point bar (sand) and channel lag (coarse residual) deposits at the point bar side of the river with channel migration. Abandoned channels are filled with sand and mud (mud plug) after avulsion or meader cut-off. Every overbank flooding event places deposits on the floodplain from proximal to distal, transitioning from sand to clay. Eroded material (crevasse splay I) deposits alongside the meander when levee breaches occur. Sediments may evolve from erosive to non-erosive (crevasse splay II) [82], and the crevasse splay channel may be added (crevasse splay channel) to the non-erosive deposits. Table A.5 provides an overview of the 9 facies model in FLUMY and their corresponding replacement in the 4-facies and 3-facies models of this study.

Appendix B. Governing equations of gas mixing

In a compositional simulation with two phases (gas and brine phases) and three components (hydrogen, methane, and brine), the dispersive flux J_i of component i represented by a concentration c is described in CMG-GEM [83] as

$$J_{i} = -\sum_{k=g,w} \phi \rho_{k} S_{k} D_{ik} \Delta c_{ik}$$
(B.1)

Table A.5Overview of the 9-facies model from FLUMY and simplified 4, 3-facies model with facies code.

Facies	9-facies	4-facies	3-facies
Channel lag	1	2 (Point bar)	2 (Point bar)
Point bar	2	2 (Point bar)	2 (Point bar)
Sand plug	3	1 (Channel)	1 (Channel)
Crevasse splay I	4	3 (Background)	3 (Background)
Crevasse splay II channel	5	3 (Background)	3 (Background)
Crevasse splay II	6	3 (Background)	3 (Background)
Levee	7	3 (Background)	3 (Background)
Overbank II	8	3 (Background)	3 (Background)
Mud plug	9	4 (Abandoned channel)	1 (Channel)

where ϕ is the porosity, ρ is the density, S is the saturation, and D denotes the dispersion tensor written as

$$D_{ik} = \begin{bmatrix} D_{ik,xx} & D_{ik,xy} & D_{ik,xz} \\ D_{ik,yx} & D_{ik,yy} & D_{ik,yz} \\ D_{ik,zx} & D_{ik,zy} & D_{ik,zz} \end{bmatrix}$$
(B.2)

where the longitudinal element $D_{ik,xx}$ (as an example) of the tensor, including the numerical dispersion [84], can be written as

$$D_{ik,xx} = \frac{D_{ik}^*}{\tau} + \alpha_L v_x + \frac{1}{2} v_x (\Delta x + v_x \Delta t)$$
(B.3)

where D_{ik}^* denotes the molecular diffusion coefficient of component i in phase k, τ is the reservoir rock tortuosity, α_L is the longitudinal dispersivity, v_x is the longitudinal velocity, Δx is the grid cell size, and Δt is the simulation time step size. A full description of governing equations and derivations can be found in [77.83,84].

In this study, the D_{ik}^* and α_L are set as zero to make the gas mixing during the simulation to only be a function of v_x which is heavily affected by the heterogeneity. This decision has been made to simplify the simulation setting and focus on the effects of multi-scale heterogeneity.

Data availability

No data was used for the research described in the article.

References

- Bo Z, Hörning S, Underschultz JR, Garnett A, Hurter S. Effects of geological heterogeneity on gas mixing during underground hydrogen storage (UHS) in braided-fluvial reservoirs. Fuel 2024;357:129949.
- [2] Jahanbakhsh A, Potapov-Crighton AL, Mosallanezhad A, Kaloorazi NT, Maroto-Valer MM. Underground hydrogen storage: A UK perspective. Renew Sustain Energy Rev 2024;189:114001.
- [3] Raza A, Mahmoud M, Arif M, Alafnan S. Underground hydrogen storage prospects in the Kingdom of Saudi Arabia. Fuel 2024;357:129665.
- [4] Wang H, Xin Y, Kou Z, Qu Y, Wang L, Ning Y, et al. Numerical study of the efficiency of underground hydrogen storage in deep saline aquifers, rock springs uplift. wvoming, J Clean Prod 2023;421:138484.
- [5] Kanaani M, Sedaee B, Asadian-Pakfar M, Gilavand M, Almahmoudi Z. Development of multi-objective co-optimization framework for underground hydrogen storage and carbon dioxide storage using machine learning algorithms. J Clean Prod 2023;386:135785.
- [6] Saadat Z, Farazmand M, Sameti M. Integration of underground green hydrogen storage in hybrid energy generation. Fuel 2024;371:131899.
- [7] Zhao Q, Guo R, Jha NK, Sarmadivaleh M, Lebedev M, Al-Yaseri A, et al. Using X-ray computed tomography and pore-scale numerical modeling to study the role of heterogeneous rock surface wettability on hydrogen-brine two-phase flow in underground hydrogen storage. Fuel 2024;366:131414.
- [8] Pan B, Song T, Yue M, Chen S, Zhang L, Edlmann K, et al. Machine learning-based shale wettability prediction: Implications for H2, CH4 and CO2 geo-storage. Int J Hydrog Energy 2024;56:1384–90.
- [9] Iglauer S, Ali M, Keshavarz A. Hydrogen wettability of sandstone reservoirs: implications for hydrogen geo-storage. Geophys Res Lett 2021;48(3):e2020GL090814.
- [10] Hashemi L, Boon M, Glerum W, Farajzadeh R, Hajibeygi H. A comparative study for H2–CH4 mixture wettability in sandstone porous rocks relevant to underground hydrogen storage. Adv Water Resour 2022;163:104165.

- [11] Hassanpouryouzband A, Adie K, Cowen T, Thaysen EM, Heinemann N, Butler IB, et al. Geological hydrogen storage: Geochemical reactivity of hydrogen with sandstone reservoirs. ACS Energy Lett 2022;7:2203–10.
- [12] Yang K, Kobeissi S, Ling N, Li M, Esteban L, May EF, et al. Measurement of hydrogen dispersion in rock cores using benchtop NMR. Int J Hydrog Energy 2023.
- [13] Kobeissi S, Ling NN, Yang K, May EF, Johns ML. Dispersion of hydrogen in different potential cushion gases. Int J Hydrog Energy 2024;60:940–8.
- [14] Boon M, Hajibeygi H. Experimental characterization of H₂/water multiphase flow in heterogeneous sandstone rock at the core scale relevant for underground hydrogen storage (UHS). Sci Rep 2022;12.
- [15] Lysyy M, Føyen T, Johannesen EB, Fernø M, Ersland G. Hydrogen Relative Permeability Hysteresis in Underground Storage. Geophys Res Lett 2022;49(17):e2022GL100364. http://dx.doi.org/10.1029/2022GL100364, URL https://onlinelibrary.wiley.com/doi/abs/10.1029/2022GL100364.
- [16] Mirchi V, Dejam M, Alvarado V, Akbarabadi M. Effect of cushion gas on hydrogen/brine flow behavior in oil-wet rocks with application to hydrogen storage in depleted oil and gas reservoirs. Energy & Fuels 2023;37(19):15231–43.
- [17] Gao J, Kong D, Peng Y, Zhou Y, Liu Y, Zhu W. Pore-scale mechanisms and hysteresis effect during multi-cycle injection and production process in underground hydrogen storage reservoir. Energy 2023;283:129007.
- [18] Zeng L, Vialle S, Ennis-King J, Esteban L, Sarmadivaleh M, Sarout J, et al. Role of geochemical reactions on caprock integrity during underground hydrogen storage. J Energy Storage 2023;65:107414.
- [19] Delshad M, Umurzakov Y, Sepehrnoori K, Eichhubl P, Batista Fernandes BR. Hydrogen storage assessment in depleted oil reservoir and saline aquifer. Energies 2022;15(21):8132.
- [20] Delshad M, Alhotan M, Fernandes B, Umurzakov Y, Sepehrnoori K. Modeling flow and transport in saline aquifers and depleted hydrocarbon reservoirs for hydrogen energy storage. SPE J 2023;28(05):2547-65.
- [21] Liu K, Zhu W, Pan B. Feasibility of hydrogen storage in depleted shale gas reservoir: A numerical investigation. Fuel 2024;357:129703.
- [22] Lysyy M, Føyen T, Johannesen EB, Fernø M, Ersland G. Hydrogen relative permeability hysteresis in underground storage. Geophys Res Lett 2022;e2022GL100364.
- [23] Higgs S, Da Wang Y, Sun C, Ennis-King J, Jackson SJ, Armstrong RT, et al. Comparative analysis of hydrogen, methane and nitrogen relative permeability: Implications for underground hydrogen storage. J Energy Storage 2023;73:108827.
- [24] Bo Z, Boon M, Hajibeygi H, Hurter S. Impact of experimentally measured relative permeability hysteresis on reservoir-scale performance of underground hydrogen storage (UHS). Int J Hydrog Energy 2023.
- [25] Pan B, Liu K, Ren B, Zhang M, Ju Y, Gu J, et al. Impacts of relative permeability hysteresis, wettability, and injection/withdrawal schemes on underground hydrogen storage in saline aquifers. Fuel 2023;333:126516.
- [26] Thaysen EM, Armitage T, Slabon L, Hassanpouryouzband A, Edlmann K. Microbial risk assessment for underground hydrogen storage in porous rocks. Fuel 2023;352:128852.
- [27] Kar SK, Sinha ASK, Bansal R, Shabani B, Harichandan S. Overview of hydrogen economy in Australia. Wiley Interdiscip Reviews: Energy Environ 2023;12(1):e457.
- [28] Bo Z, Zeng L, Chen Y, Xie Q. Geochemical reactions-induced hydrogen loss during underground hydrogen storage in sandstone reservoirs. Int J Hydrog Energy 2021;46(38):19998–20009.
- [29] Bensing JP, Misch D, Skerbisch L, Sachsenhofer RF. Hydrogen-induced calcite dissolution in amaltheenton formation claystones: Implications for underground hydrogen storage caprock integrity. Int J Hydrog Energy 2022;47(71):30621-6.
- [30] Thaysen EM, McMahon S, Strobel GJ, Butler IB, Ngwenya BT, et al. Estimating microbial growth and hydrogen consumption in hydrogen storage in porous media. Renew Sustain Energy Rev 2021;151:111481.
- [31] Liu N, Kovscek AR, Fernø MA, Dopffel N. Pore-scale study of microbial hydrogen consumption and wettability alteration during underground hydrogen storage. Front Energy Res 2023;11:1124621.
- [32] Okoroafor ER, Saltzer SD, Kovscek AR. Toward underground hydrogen storage in porous media: Reservoir engineering insights. Int J Hydrog Energy 2022.
- [33] Tarkowski R, Uliasz-Misiak B. Towards underground hydrogen storage: A review of barriers. Renew Sustain Energy Rev 2022;162:112451.
- [34] Hassanpouryouzband A, Joonaki E, Edlmann K, Haszeldine RS. Offshore geological storage of hydrogen: Is this our best option to achieve net-zero? ACS Energy Lett 2021;6(6):2181–6.
- [35] Zeng L, Sander R, Chen Y, Xie Q. Hydrogen storage performance during underground hydrogen storage in depleted gas reservoirs: A review. Engineering 2024.
- [36] Kumar KR, Honorio H, Chandra D, Lesueur M, Hajibeygi H. Comprehensive review of geomechanics of underground hydrogen storage in depleted reservoirs and salt caverns. J Energy Storage 2023;73:108912.
- [37] Boon M, Buntic I, Ahmed K, Dopffel N, Peters C, Hajibeygi H. Microbial induced wettability alteration with implications for underground hydrogen storage. Sci Rep 2024;14(1):8248.

[38] Kumar KR, Hajibeygi H. Multiscale simulation of inelastic creep deformation for geological rocks. J Comput Phys 2021;440:110439.

- [39] Al-Yaseri A, Amao A, Fatah A. Experimental investigation of shale/hydrogen geochemical interactions. Fuel 2023;346:128272.
- [40] Raza A, Arif M, Glatz G, Mahmoud M, Al Kobaisi M, Alafnan S, et al. A holistic overview of underground hydrogen storage: Influencing factors, current understanding, and outlook. Fuel 2022;330:125636.
- [41] Saeed M, Jadhawar P. Modelling underground hydrogen storage: A state-of-the-art review of fundamental approaches and findings. Gas Sci Eng 2023:205196
- [42] Yang Y, Yin X, Yang Y, Tian H, Liu K, Zhu W, et al. Numerical simulations of depleted (CH4) and cushion (CO2) gases impacts on H2 withdrawal and CO2 storage efficiencies in a depleted gas reservoir. Fuel 2025;380:133095.
- [43] Carrera J, Saaltink MW, Soler-Sagarra J, Wang J, Valhondo C. Reactive transport: a review of basic concepts with emphasis on biochemical processes. Energies 2022;15(3):925.
- [44] Feldmann F, Hagemann B, Ganzer L, Panfilov M. Numerical simulation of hydrodynamic and gas mixing processes in underground hydrogen storages. Environ Earth Sci 2016;75(16):1165, Publisher: Springer.
- [45] Lysyy M, Fernø M, Ersland G. Seasonal hydrogen storage in a depleted oil and gas field. Int J Hydrog Energy 2021;46(49):25160–74. http://dx.doi.org/10.1016/ j.ijhydene.2021.05.030, URL https://www.sciencedirect.com/science/article/pii/ S0360319921017444.
- [46] SEAL Energy. A petrophysical model of the Waarre Formation in the Port Campbell Embayment. Technical Report Victorian Gas Program Technical Report 17, Geological Survey of Victoria; 2020.
- [47] Amirthan T, Perera M. Underground hydrogen storage in Australia: a review on the feasibility of geological sites. Int J Hydrog Energy 2023;48(11):4300–28.
- [48] Bo Z. Extending the life of gas fields by re-purposing for hydrogenstorage to support Australia's energy transition. Univ Qld 2024. http://dx.doi.org/10. 14264/6285fda.
- [49] Cadman S, Pain L, Vuckovic V. Bowen and surat basins, clarence-moreton basin, sydney basin, gunnedah basin and other minor onshore basing, qld, NSW and NT. Department of Primary Industries and Energy, Bureau of Resource Sciences; 1997.
- [50] Cinar Y, Neal PR, Allinson WG, Sayers J. Geoengineering and economic assessment of a potential carbon capture and storage site in southeast queensland, Australia. SPE Reserv Eval Eng 2009;12(05):660–70.
- [51] Jones A, Doyle J, Jacobsen T, Kjønsvik D. Which sub-seismic heterogeneities influence waterflood performance? A case study of a low net-to-gross fluvial reservoir. Geol Soc Lond Spec Publ 1995;84(1):5–18, Publisher: Geological Society of London.
- [52] Jordan DW, Pryor WA. Hierarchical levels of heterogeneity in a Mississippi River meander belt and application to reservoir systems. AAPG Bull 1992;76(10):1601–24, Publisher: American Association of Petroleum Geologists (AAPG).
- [53] Slatt RM. Fluvial deposits and reservoirs. In: Developments in petroleum science, vol. 61, Elsevier; 2013, p. 283–369.
- [54] Willis BJ, Tang H. Three-dimensional connectivity of point-bar deposits. J Sediment Res 2010;80(5):440–54.
- [55] Sun T, Meakin P, Jøssang T. A computer model for meandering rivers with multiple bed load sediment sizes: 1. Theory. Water Resour Res 2001;37(8):2227–41.
- [56] Burns CE, Mountney N, Hodgson D, Colombera L. Anatomy and dimensions of fluvial crevasse-splay deposits: Examples from the cretaceous castlegate sandstone and neslen formation, utah, USA. Sediment Geol 2017;351:21–35.
- [57] Miall AD. The geology of fluvial deposits: sedimentary facies, basin analysis, and petroleum geology. Springer; 2013.
- [58] Colombera L, Mountney NP, Russell CE, Shiers MN, McCaffrey WD. Geometry and compartmentalization of fluvial meander-belt reservoirs at the bar-form scale: Quantitative insight from outcrop, modern and subsurface analogues. Mar Pet Geol 2017;82:35–55.
- [59] Berg RR. Point-bar origin of fall river sandstone reservoirs, northeastern wyoming. AAPG Bull 1968;52(11):2116–22.
- [60] Larue DK, Hovadik J. Connectivity of channelized reservoirs: a modelling approach. Pet Geosci 2006;12(4):291–308.
- [61] Montero JM, Colombera L, Yan N, Mountney NP. A workflow for modelling fluvial meander-belt successions: Combining forward stratigraphic modelling and multi-point geostatistics. J Pet Sci Eng 2021;201:108411.
- [62] Sun C, Demyanov V, Arnold D. Geological realism in fluvial facies modelling with GAN under variable depositional conditions. Comput Geosci 2023;27(2):203–21.
- [63] Li J, Lin C, Zhang X, Dong C, Wei Y, Ning W, et al. Multiscale modeling of meandering fluvial reservoir architecture based on multiple-point geostatistics: a case study of the minghuazhen formation, yangerzhuang oilfield, Bohai Bay Basin, China. Geofluids 2021;2021:1–17.
- [64] Koneshloo M, Aryana SA, Hu X. The impact of geological uncertainty on primary production from a fluvial reservoir. Pet Sci 2018;15:270–88.
- [65] Hovorka SD, Doughty C, Benson SM, Pruess K, Knox PR. The impact of geological heterogeneity on CO2 storage in brine formations: a case study from the texas Gulf Coast. Geol Soc Lond Spec Publ 2004;233(1):147–63.

- [66] Cojan I, Fouché O, Lopéz S, Rivoirard J. Process-based reservoir modelling in the example of meandering channel. Geostat Banff 2004 2005;611–9.
- [67] Colombera L, Mountney NP, McCaffrey WD. A quantitative approach to fluvial facies models: methods and example results. Sedimentology 2013;60(6):1526–58.
- [68] Gibling MR. Width and thickness of fluvial channel bodies and valley fills in the geological record: a literature compilation and classification. J Sediment Res 2006;76(5):731–70, Publisher: SEPM Society for Sedimentary Geology.
- [69] Xue P. A point bar facies reservoir model-semi-communicated sandbody. In: SPE international oil and gas conference and exhibition in China. SPE; 1986, p. SPE-14837.
- [70] La Croix AD, Wang J, He J, Hannaford C, Bianchi V, Esterle J, et al. Widespread nearshore and shallow marine deposition within the lower jurassic precipice sandstone and evergreen formation in the surat basin, Australia. Mar Pet Geol 2019;109:760-90
- [71] Brelih D, Kodl E. Detailed mapping of fluvial sand bodies improves perforating strategy at kern river field. In: SPE western regional meeting. SPE; 1990, p. SPE-20080.
- [72] Hastings JO. Coarse-grained meander-belt reservoirs, rocky ridge field, north dakota. Sandstone Pet Reserv 1990;57–84.
- [73] SEAL Energy. Dynamic modelling workflow for the Underground Gas Storage project, Onshore Otway Basin. Technical Report Victorian Gas Program Technical Report 41. Geological Survey of Victoria. Department of Jobs: 2020.
- [74] Ershadnia R, Hajirezaie S, Amooie A, Wallace CD, Gershenzon NI, Hosseini SA, et al. CO2 geological sequestration in multiscale heterogeneous aquifers: Effects of heterogeneity, connectivity, impurity, and hysteresis. Adv Water Resour 2021;151:103895.

- [75] Aziz K. Petroleum reservoir simulation. Appl Sci Publ 1979;476.
- [76] Zamehrian M, Sedaee B. Underground hydrogen storage in a partially depleted gas condensate reservoir: Influence of cushion gas. J Pet Sci Eng 2022;212:110304, Publisher: Elsevier.
- [77] Garmeh G, Johns RT. Upscaling of miscible floods in heterogeneous reservoirs considering reservoir mixing. SPE Reserv Eval Eng 2010;13(05):747–63.
- [78] Farajzadeh R, Ranganathan P, Zitha P, Bruining J. The effect of heterogeneity on the character of density-driven natural convection of CO2 overlying a brine layer. Adv Water Resour 2011;34(3):327–39.
- [79] Møyner O, Krogstad S, Lie K-A. The application of flow diagnostics for reservoir management. SPE J 2015;20(02):306–23.
- [80] Lie K-A. An introduction to reservoir simulation using MATLAB/GNU Octave: User guide for the MATLAB Reservoir Simulation Toolbox (MRST). Cambridge University Press; 2019.
- [81] Gasanzade F, Pfeiffer WT, Witte F, Tuschy I, Bauer S. Subsurface renewable energy storage capacity for hydrogen, methane and compressed air–a performance assessment study from the north german basin. Renew Sustain Energy Rev 2021:149:111422.
- [82] Sun C, Demyanov V, Arnold D. GAN river-I: A process-based low NTG meandering reservoir model dataset for machine learning studies. Data Brief 2023;46:108785.
- [83] Computer Modeling Group. User's guide gem, advanced compositional reservoir simulator (version 2020). computer modeling group ltd, calgary.. Computer Modeling Group; 2020, URL https://www.cmgl.ca/gem.
- [84] Fanchi JR. Multidimensional numerical dispersion. Soc Pet Eng J 1983;23(01):143–51.